Available online at www.sciencedirect.com
SCIENCE DIRECT®
International Journal of Solids and Structures 42 (2005) 1831–1846
INTERNATIONAL JOURNAL OF SOLIDS and STRUCTURES
www.elsevier.com/locate/ijsolstr

Correcting power-law viscoelastic effects in elastic modulus measurement using depth-sensing indentation

A.H.W. Ngan *, H.T. Wang [1], B. Tang, K.Y. Sze

Department of Mechanical Engineering, The University of Hong Kong, Pokfulam Road, Hong Kong, PR China

Received 8 October 2003; received in revised form 22 July 2004
Available online 25 September 2004

Abstract

The standard Oliver–Pharr method for measuring the elastic modulus by depth-sensing indentation makes use of the unloading response of the material as it is assumed that the unloading behaviour is purely elastic. However, under certain conditions, the unloading behaviour can be viscoelastic, and if the viscosity effects are not corrected, the calculated modulus can be seriously erroneous. Feng and Ngan have proposed a correction formula which can eliminate the creep effects. However, this formula has been proven to be correct for the case of linear viscoelasticity only; the general case of power-law viscoelasticity has not been proven. In this paper, this formula is proved for the general power-law viscoelastic situation using a Maxwell material model. Finite-element calculations are also performed to illustrate the result. The correction formula is applied to experimental data on amorphous selenium at ambient and elevated temperatures and is found to be effective in correcting for creep effects which are very prominent in this material.

Keywords: Mechanical properties; Nanoindentation; Elasticity; Creep; Hardness testing

1. Introduction

Depth-sensing indentation has become a standard technique for the measurement of the elastic modulus of small samples. In the well-known Oliver–Pharr method for modulus measurement (Oliver and Pharr, 1992), the reduced modulus E_r, defined as

* Corresponding author. Tel.: +852 2859 7900; fax: +852 2858 5415.
E-mail address: hwngan@hku.hk (A.H.W. Ngan).
[1] On leave from: Department of Civil Engineering, South China University of Technology, Guangzhou 510640, PR China.

0020-7683/$ - see front matter © 2004 Elsevier Ltd. All rights reserved.
doi:10.1016/j.ijsolstr.2004.07.018

$$\frac{1}{E_r} = \left(\frac{1-v^2}{E}\right)_{\text{sample}} + \left(\frac{1-v^2}{E}\right)_{\text{indenter}} \tag{1}$$

is calculated from the contact stiffness S using the following formula which is derived from Sneddon's solution (Sneddon, 1965) to the elastic contact problem between a half space and an axi-symmetric punch:

$$E_r = \frac{\sqrt{\pi}}{2}\frac{S}{\sqrt{A_c}}. \tag{2}$$

Here v and E are Poisson's ratio and Young's modulus, and A_c is the tip–sample contact area at full load P_{max}. The contact area A_c is calculated from the contact depth h_c through a pre-calibrated shape function $A_c = f(h_c)$ of the indenter, and h_c is given by

$$h_c = h_{max} - \varepsilon\frac{P_{max}}{S}, \tag{3}$$

where h_{max} is the maximum indenter displacement, and ε is a constant depending on the indenter geometry ($\varepsilon = 0.72$ for the Berkovich tip).

Eq. (2) was derived based on the assumption that the material behaviour is purely elastic. However, many experiments have indicated that creep effects usually occur during nanoindentation (Mayo and Nix, 1988; LaFontaine et al., 1990; Baker et al., 1992; Ramman and Berriche, 1992; O'Connor and Cleveland, 1993; Syed and Pethica, 1997; Lucas and Oliver, 1999; Feng and Ngan, 2001a,b; Ngan and Tang, 2002; Li and Ngan, 2004). In low-melting metals, indentation creep can occur before general yield (Feng and Ngan, 2001a,b) but for high-melting metals, crystal plasticity is a pre-requisite condition for indentation creep (Syed and Pethica, 1997; Feng and Ngan, 2001a,b). In extreme creeping situations, the unloading curve can exhibit a "nose", meaning that the indenter can continue to sink into the specimen even though the load is decreasing. The conditions for the occurrence of unloading "nose" have been investigated by Ngan and Tang (2002). Recently, it has also been demonstrated that the stress exponent of nanoindentation creep exhibits a strong dependence on the indent size (Li and Ngan, 2004), indicating a transition of creep mechanism as indent size approaches the incipient plasticity situation.

On the specific question of how indentation creep affects the calculated modulus, a number of reports have indicated that the measured modulus can be seriously affected by creep (Chudoba and Richter, 2001; Feng and Ngan, 2001a,b; Feng and Ngan, 2002; Tang and Ngan, 2003). Summarising these findings, indentation creep will exert significant effects on the measured modulus when (i) the material itself is low-melting or soft, (ii) the load hold before unloading is too brief, (iii) the unloading rate is too slow, and (iv) the full load is too large. For reasonably hard materials like metals or ceramics at testing temperatures low compared to their melting points, the effects of creep can be eliminated by using an extended load hold or a rapid unloading rate, as is perhaps well-known. However, for soft materials like polymers or biological tissues, or if the aim of the experiment is to deliberately measure the elastic modulus at a high temperature compared to the melting point, the load hold or the unloading rate required to eliminate creep effects may be difficult to achieve in practice. Ngan and co-workers (Feng and Ngan, 2001a,b, 2002; Tang and Ngan, 2003) have developed correction formulas to eliminate creep effects in the post-experiment, data-processing stage. It was proposed that, in a viscoelastic situation, the correct elastic stiffness S_e can be calculated as

$$\frac{1}{S_e} = \frac{1}{S} - \frac{\dot{h}_h}{\dot{P}_u}, \tag{4}$$

where S is the apparent contact stiffness dP/dh at the onset of unloading (P = load, h = indenter displacement), $\dot{h}_h$ is the tip displacement rate at the end of the load hold just prior to unloading, and $\dot{P}_u$ is the

unloading rate. The S_e calculated this way should replace S in Eq. (2). Tang and Ngan (2003) have further proposed that the Oliver–Pharr Eq. (3) in the viscoelastic situation should be replaced by

$$h_c = h_{max} - \varepsilon \frac{P_{max}}{S_e} = h_{max} - \varepsilon P_{max}\left(\frac{1}{S} - \frac{\dot{h}_h}{\dot{P}_u}\right). \tag{5}$$

Compared to the Oliver–Pharr method, the method described by Eqs. (4) and (5) involves the measurement of the additional parameter $\dot{h}_h$ ($\dot{P}_u$ is a prescribed quantity). Here, $\dot{h}_h$ can be conveniently measured by monitoring the creep behaviour during the load hold period prior to unloading. In their first paper, Feng and Ngan (2001a,b) explained Eq. (4) using a "superposition" approximation in which the overall indenter displacement h at any time is the sum of a creep component and an elastic component, and each of these satisfies their own constitutive law. The same superposition approximation was used to derive Eq. (5) by Tang and Ngan (2003). The superposition assumption is of course only a phenomenological approximation and in their second paper, Feng and Ngan (2002) gave a formal proof of Eq. (4) in the situation of linear viscoelasticity for a Maxwell spring-dashpot material model. The approach they used was the "correspondence principle" which is only applicable to linear viscoelasticity (Sakai, 2002).

Eq. (4) has not been proven for the general situation of power-law viscoelasticity. Furthermore, Eq. (5) has never been rigorously proven beyond the superposition approximation as mentioned above, although it must be remembered that the original Oliver–Pharr Eq. (3) was also derived along a similar line involving the superposition approximation and has similarly never been proven beyond such an approximation. Eq. (3) is known to significantly underestimate the contact size if pile-up occurs around the indent (McElhaney et al., 1998). In spite of this, the available experimental data on a range of materials (Feng and Ngan, 2001a,b, 2002; Tang and Ngan, 2003) seem to indicate that application of Eqs. (4) and (5) can effectively correct for creep effects in modulus measurement.

The purpose of this paper is to prove Eq. (4) for the general situation of power-law viscoelasticity. From the above, it is clear that Eq. (5) is only an approximation and therefore no attempt is made to rigorously prove its correctness. However, simulations by the finite element method (FEM) are performed in this work to investigate the validity of Eq. (5) in different power-law viscoelastic situations. Finally, we also present ambient and elevated-temperature experimental results on selenium to illustrate the conclusions. We choose selenium because this material is known to exhibit significant power-law creep at ambient temperature.

2. Proof of correction formula for stiffness measurement

Consider the situation in which a half-space is deformed by a blunt indenter under load P as shown in Fig. 1. The instantaneous contact area at time t has a radius a, and the indentation depth is h. We prescribe a Cartesian coordinate system x_k ($k = 1$–3) such that x_3 is along the indentation axis and $x_3 = 0$ marks the surface of the half-space $x_3 \geqslant 0$. We assume the material occupying the half-space has a Maxwell-type

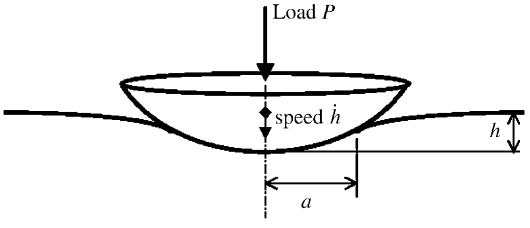

Fig. 1. Indentation into a half-space.

viscoelastic behaviour, in which the elastic strain and the creep strain are additive. The stress–strain relation is given by

$$\dot{\varepsilon}_{ij} = \frac{3}{2}\dot{\varepsilon}_{\mathrm{o}}\left(\frac{\sigma_{\mathrm{e}}}{\sigma_{\mathrm{o}}}\right)^{m-1}\frac{S_{ij}}{\sigma_{\mathrm{o}}} + s_{ijkl}\dot{\sigma}_{kl}, \tag{6}$$

where, as before, $\dot{(\,)} = \partial()/\partial t$ (t = time), $S_{ij} = \sigma_{ij} - \frac{\delta_{ij}}{3}\sigma_{kk}$ is the deviatoric stress, $\sigma_{\mathrm{e}} = \sqrt{\frac{3}{2}S_{ij}S_{ij}}$, s_{ijkl} is the elastic compliance matrix, $\dot{\varepsilon}_{\mathrm{o}}$ and σ_{o} are material creep parameters with dimensions of strain-rate and stress respectively, and m is the stress exponent. In Eq. (6), the first term is the creep component and the second the elastic component. We consider a typical load schedule consisting of a load-hold period followed immediately by an unloading period as shown in Fig. 2. The instant of the commencement of unloading is denoted as t_{h}.

At the instants $t = t_{\mathrm{h}}^-$ just prior to unloading and $t = t_{\mathrm{h}}^+$ just after unloading has begun, the strain rate fields are given by Eq. (6) as

$$\dot{\varepsilon}_{ij}(t_{\mathrm{h}}^-) = \frac{3}{2}\dot{\varepsilon}_{\mathrm{o}}\left(\frac{\sigma_{\mathrm{e}}(t_{\mathrm{h}})}{\sigma_{\mathrm{o}}}\right)^{m-1}\frac{S_{ij}(t_{\mathrm{h}})}{\sigma_{\mathrm{o}}} + s_{ijkl}\dot{\sigma}_{kl}(t_{\mathrm{h}}^-) \quad \text{at } t = t_{\mathrm{h}}^-, \tag{7}$$

$$\dot{\varepsilon}_{ij}(t_{\mathrm{h}}^+) = \frac{3}{2}\dot{\varepsilon}_{\mathrm{o}}\left(\frac{\sigma_{\mathrm{e}}(t_{\mathrm{h}})}{\sigma_{\mathrm{o}}}\right)^{m-1}\frac{S_{ij}(t_{\mathrm{h}})}{\sigma_{\mathrm{o}}} + s_{ijkl}\dot{\sigma}_{kl}(t_{\mathrm{h}}^+) \quad \text{at } t = t_{\mathrm{h}}^+. \tag{8}$$

Note that in the above, we denote the stress fields at both instants of $t = t_{\mathrm{h}}^-$ and $t = t_{\mathrm{h}}^+$ as $\sigma_{ij}(t_{\mathrm{h}})$, $\sigma_{\mathrm{e}}(t_{\mathrm{h}})$, and $S_{ij}(t_{\mathrm{h}})$, i.e. the stress fields at both instants are the same. This is so because the stress fields have to be continuous from $t = t_{\mathrm{h}}^-$ to $t = t_{\mathrm{h}}^+$, since the load P is continuous during this transition. What is discontinuous at t_{h} is the loading rate $\dot{P}$, which is zero at $t = t_{\mathrm{h}}^-$ and negative at $t = t_{\mathrm{h}}^+$. This discontinuity will cause corresponding discontinuities in the strain rate and stress rate fields $\dot{\varepsilon}_{ij}$ and $\dot{\sigma}_{ij}$, and hence, $\dot{\varepsilon}_{ij}$ and $\dot{\sigma}_{ij}$ are marked as differently between Eqs. (7) and (8). The jump in strain rate across t_{h} is given by subtracting Eq. (7) from Eq. (8), viz

$$\Delta\dot{\varepsilon}_{ij} = \dot{\varepsilon}_{ij}(t_{\mathrm{h}}^+) - \dot{\varepsilon}_{ij}(t_{\mathrm{h}}^-) = s_{ijkl}\Delta\dot{\sigma}_{kl}, \tag{9}$$

where $\Delta\dot{\sigma}_{ij} = \dot{\sigma}_{ij}(t_{\mathrm{h}}^+) - \dot{\sigma}_{ij}(t_{\mathrm{h}}^-)$ is the jump in stress rate across t_{h}. The strain ε_{ij} is associated with the displacement u_i through $\varepsilon_{ij} = (u_{i,j} + u_{j,i})/2$, so that $\Delta\dot{\varepsilon}_{ij}$ is associated with the jump in velocity $\Delta\dot{u}_i = \dot{u}_i(t_{\mathrm{h}}^+) - \dot{u}_i(t_{\mathrm{h}}^-)$ through

$$\Delta\dot{\varepsilon}_{ij} = (\Delta\dot{u}_{i,j} + \Delta\dot{u}_{j,i})/2. \tag{10}$$

Eqs. (9) and (10) indicate that $\{\Delta\dot{u}_i, \Delta\dot{\varepsilon}_{ij}, \Delta\dot{\sigma}_{ij}\}$ may be regarded as the {displacement, strain, stress} of a linear elastic problem, defined on the same half-space $x_3 \geqslant 0$ as the original specimen, and possessing the same elastic compliance s_{ijkl} as well. The boundary conditions for the $\{\Delta\dot{u}_i, \Delta\dot{\varepsilon}_{ij}, \Delta\dot{\sigma}_{ij}\}$ problem are

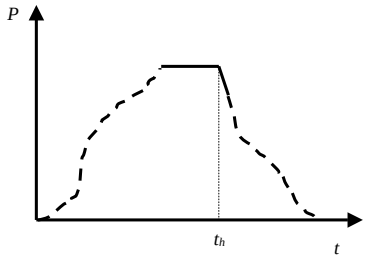

Fig. 2. A general load schedule consisting of a load hold followed by unload.

$$\Delta\dot{u}_3 = \Delta\dot{h} = \dot{h}_u - \dot{h}_h \text{ for } r = \sqrt{x_1^2 + x_2^2} \leqslant a,\ x_3 = 0, \tag{11a}$$

$$\Delta\dot{\sigma}_{3k} = 0, \quad k = 1,2,3, \text{ for } r = \sqrt{x_1^2 + x_2^2} > a,\ x_3 = 0, \tag{11b}$$

and

$$\Delta\dot{u}_k = 0, \quad k = 1,2, \text{ for } r = \sqrt{x_1^2 + x_2^2} \leqslant a,\ x_3 = 0 \text{ for a sticking tip}, \tag{11c}$$

or

$$\Delta\dot{\sigma}_{3k} = 0, \quad k = 1,2, \text{ for } r = \sqrt{x_1^2 + x_2^2} \leqslant a,\ x_3 = 0 \text{ for a smooth tip}. \tag{11d}$$

In Eq. (11a), $\dot{h}_u = \dot{h}(t_h^+)$ and $\dot{h}_h = \dot{h}(t_h^-)$ and so $\Delta\dot{h}$ is the jump in the tip displacement rate across t_h. Eqs. (9–11) are equivalent to the indentation problem by a rigid, cylindrical flat-ended punch into an elastic half-space, such that the punch displacement has a magnitude equal to $\Delta\dot{h}$. This problem is depicted in Fig. 3, and the flat-punch indentation problem in general has been solved by Sneddon for the case of isotropic elasticity (Sneddon, 1965). In particular, Sneddon has shown that the relation between the indentation force P and indenter displacement D in the flat-punch problem is given by (see Eq. (6.1) in Sneddon, 1965)

$$P = \frac{2EaD}{1 - \nu^2}. \tag{12}$$

In the original indentation problem in Fig. 1, the indentation load P is given by

$$P = 2\pi \int_0^a \sigma_{33}(r, x_3 = 0) r\,\mathrm{d}r. \tag{13}$$

From this, the jump in the load rate from $\dot{P}_h = \dot{P}(t_h^-)$ to $\dot{P}_u = \dot{P}(t_h^+)$ across t_h can be obtained as

$$\dot{P}_u - \dot{P}_h = -2\pi \int_0^a \Delta\dot{\sigma}_{33}(r, x_3 = 0) r\,\mathrm{d}r. \tag{14}$$

From the Sneddon solution to the $\{\Delta\dot{u}_i, \Delta\dot{\varepsilon}_{ij}, \Delta\dot{\sigma}_{ij}\}$ flat-punch problem defined by Eqs. (9–11), the right hand side of Eq. (14) is in fact equal to the right hand side of Eq. (12) with the substitution $D = \Delta\dot{h}$. Therefore, Eq. (14) becomes

$$\dot{P}_u - \dot{P}_h = 2aE_r(\dot{h}_u - \dot{h}_h), \tag{15}$$

where $E_r = E/(1-\nu^2)$ is the reduced modulus defined in Eq. (1) for the case of rigid indenter. For an elastic indenter, the "elastic" problem presented in Eqs. (9–11) needs to be solved as a contact problem between an elastic half space and an elastic flat punch. Earlier works (Pharr et al., 1992) have shown that in this

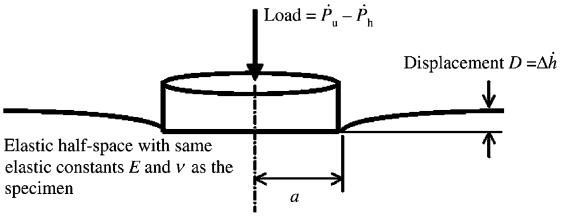

Fig. 3. The equivalent flat-punch indentation problem into the same elastic half-space as the specimen.

situation, Sneddon's Eq. (12) still holds except that E_r is now given by Eq. (1) containing the indenter's elastic constants.

Eq. (4) follows directly from Eq. (15) by noting $S_e = 2aE_r$, $S = \dot{P}_u/\dot{h}_u$, and $\dot{P}_h = 0$. The condition of $\dot{P}_h = 0$ is valid only in an ideal load-hold condition; in actual load-hold experiments on severely creeping materials, the significant creep displacement may lead to a large restoring force in the springs on which the indenter tip is suspended in a typical depth-sensing instrument, and hence the actual load applied onto the specimen may be decreasing with time (Feng and Ngan, 2001a,b). In some setup, this problem can be alleviated by a feedback loop which increases the set-point load as tip displacement increases to compensate for the increasing spring force, but more often, the spring force problem may be left unattended. In the latter scenario, the more general Eq. (15), which can be rewritten as

$$\frac{1}{S_e} = \left(\frac{1}{S} - \frac{\dot{h}_h}{\dot{P}_u}\right)\frac{1}{(1 - \dot{P}_h/\dot{P}_u)} \tag{16}$$

in a form comparable to Eq. (4), should be used to correct for the creep effects. To use Eq. (16), the load decaying speed $\dot{P}_h$ at $t = t_h^-$ needs to be measured as well as the creep rate $\dot{h}_h$.

It should be noted that the derivation of Eq. (15) here is very general and is, for example, independent of whether pile-up or sink-in occurs around the indentation. This is because pile-up or sink-in is allowed to occur as appropriate as dictated by the solution of the governing Eq. (6). Also, the boundary condition in Eq. (11a) for $\Delta\dot{u}_3$ will be valid for any blunt indenter shape, and so Eq. (15) should be valid for any indenter shape as long as it is blunt. Also, Eq. (11a) does not involve the datum of the displacement u_i, and hence, within the small-strain approximation, the initial shape of the free surface does not matter as long as it is slowly varying. Hence, the history prior to the moment when Eq. (6) starts to become valid does not matter. In other words, the analysis here for the behaviour around t_h will be valid if a plastic indentation is made, for example, during the rapid loading schedule prior to the load hold. In the next section, FEM calculations will be used to show the validity of Eq. (15) in different situations with pile-up, sink-in or pre-existing plastic indentation.

3. Finite element simulations

The purpose of the FE simulations here is to verify Eqs. (4) and (5) in different situations of material properties. The FE calculations were performed using the MSC.Marc package (Version 2000) with a material model described by Eq. (6). The indenter used was a conical indenter with a semi-angle of 70.3° at the apex. This geometry has the same area function as the often used Berkovich pyramidal indenter, namely, $A_c = 24.5h_c^2$. The following stress exponent values were used to investigate a wide range of material behaviour from linear creep to ideal plasticity: $m = 1$, 5, 10, 30, 50, 100. The material parameter $E\dot{\varepsilon}_o/\sigma_o$ was varied within the range from 1×10^{-18} (effectively zero) to $10\,s^{-1}$ (where σ_o is set to be 1 unit in every case) to study a wide extent of creep speed. In all calculations the Poisson's ratio was fixed at 0.3. The calculations were performed using the small-strain assumption. Owing to its unconditional stability, the implicit time integration scheme is chosen for tracing the viscoelasticity material response. To ensure that the employed time step is sufficiently fine, the time step setting is successively reduced by half until the difference of the indentation depths predicted by using two consecutive time step settings at the onset of unloading is within 1%. On the other hand, the mesh density at the contact zone is successively doubled until the difference of the computed E from Eq. (16) yielded by two consecutive mesh densities is within 1%.

Different unloading rates were also used to generate a range of apparent unloading stiffness $S = dP/dh$ between positive and negative values. Fig. 4(a) shows two simulated load–displacement curves with a negative value of S (when $m = 1$) and a nearly infinite value of S (when $m = 10$). The corresponding creep

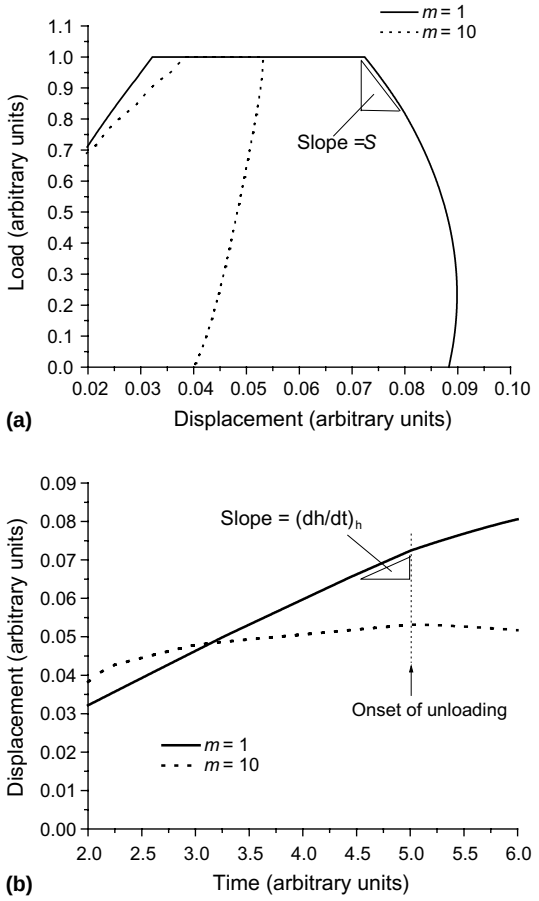

Fig. 4. Representative FE simulated load–displacement curves (a) and displacement–time curves during load hold (b). $\dot{\varepsilon}_o = 0.01$, $\dot{P}_u = -0.2$, $E/\sigma_o = 100$, all arbitary units commensurate with data in Tables 1–4.

curves during load hold are shown in Fig. 4(b). It was also noted that at small values of m, sink-in occurs, but as m increases, the free surface transits to the pile-up situation, in agreement with earlier FE simulations (Bower et al., 1993). Fig. 5(a) and (b) show the typical surface topography of the sink-in and pile-up behaviour respectively at two different values of m. Tables 1–4 show the detailed numerical results from a representative set of simulations. Here, the parameters are presented in an arbitrary set of units, i.e. σ_o is set to 1 unit of stress and E is in multiples of σ_o, lengths (h_c, a, etc.) are quoted in an arbitrary unit, and so is time. To verify Eq. (4), the creep speed just prior to unloading, $\dot{h}_h$, was calculated from the simulated displacement vs time data for each situation. The Young's modulus was calculated by first calculating S_e from Eq. (4), followed by substituting this for S in Eq. (2). The contact radius a here (see Fig. 1) was found directly from the simulated surface topography instead of using Eq. (5), so that the results reveal only the accuracy of Eq. (4) but not Eq. (5). Tables 1–4 show the simulated E at different input conditions. It can be seen that in all simulated cases, the input Young's modulus value and the calculated value differ at most by a few %, and this difference is likely to be due to numerical uncertainties. In most cases, a pre-existing indent was generated beforehand but this was not done in some cases to illustrate any difference. It can be seen from Table 1 that whether a pre-existing indent is present or not does not affect the agreement between the input and calculated Young's modulus values. Therefore, Eq. (4) is verified.

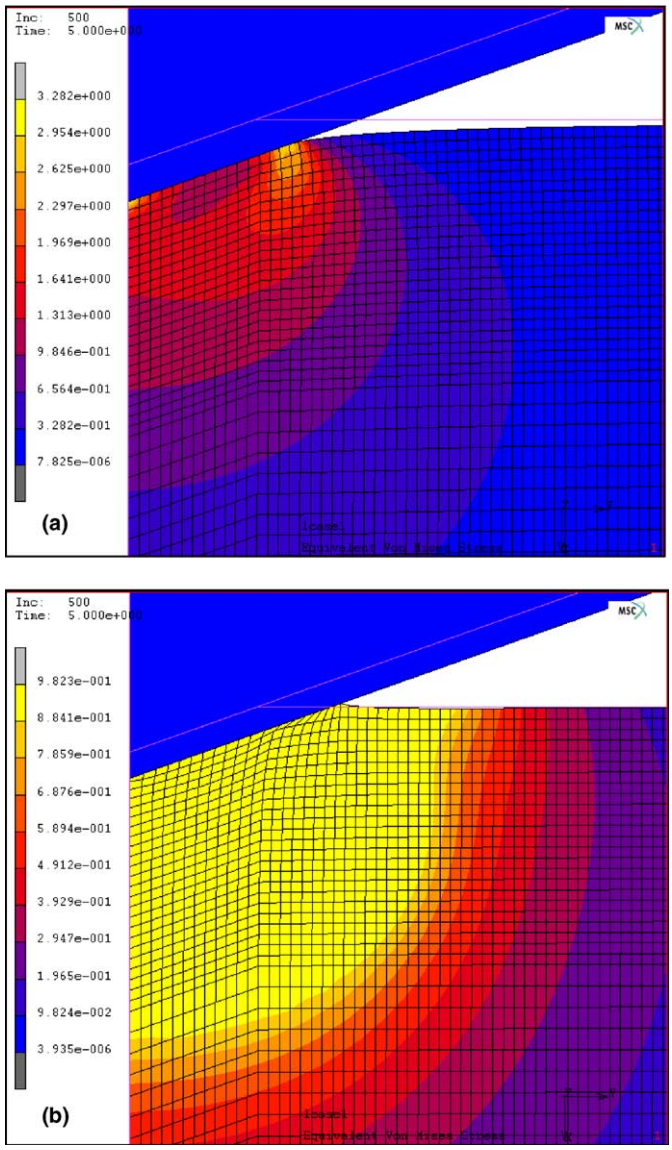

Fig. 5. FE simulated indent topography at peak load showing (a) the sink-in behaviour at $m = 1$, and (b) the pile-up behaviour at $m = 100$. $E/\sigma_o = 100$, $\dot{\varepsilon}_o = 0.01\ s^{-1}$. The upper left triangle is the indenter. The scale bars show the von Mises stress magnitudes.

Also shown in Tables 1–4 are the contact depth h_c calculated using Eq. (5). Comparing with the value observed from the simulated surface topography, it can be seen that Eq. (5) predicts fairly accurately the observed contact depth in most cases, except the case when $\dot{\varepsilon}_o$ is large at 0.1 and m is small at 1, where the error is quite severe. In other words, Eq. (5) is accurate except when creep is really fast with a small stress exponent. However, the results in Tables 1–3 show that even in this case, the h_c predicted by Eq. (5) is still closer to the real h_c than that predicted by the Oliver–Pharr Eq. (3). The results in Table 2 also show that at small m values (say <10), both the Oliver–Pharr Eq. (3) and the creep-correcting Eq. (5) overestimate h_c. However, the h_c from Eq. (5) is in closer agreement with the real h_c, which suggests that the

Table 1
Computed finite-element results at different material parameters

$\dot{\varepsilon}_o$		10^{-1}	10^{-2}	10^{-5}	10^{-10}	10^{-20}
$m = 1$	S	−4.03676	−20.9876	59.4027	59.1274	59.1274
	a	0.785701	0.315393	0.249425	0.249420	0.249420
	$\dot{h}_h$	0.0506848	0.0122893	1.56800×10^{-5}	0.000000	0.000000
	E	101.593	104.544	107.860	107.862	107.862
	h_c[a]	0.281351	0.112939	0.0893165	0.0893147	0.0893147
	h_c[b]	0.603126	0.195757	0.0934908	0.0933710	0.0933710
	h_c[c]	0.418947	0.151100	0.0934338	0.0933710	0.0933710
$m = 100$	S	95.8732	92.6295	89.8500	83.3169	74.3482
	a	0.415229	0.412760	0.391148	0.366134	0.319228
	$\dot{h}_h$	1.16917×10^{-4}	4.39040×10^{-5}	9.50680×10^{-5}	5.12500×10^{-5}	6.98840×10^{-5}
	E	99.4805	100.074	100.236	101.375	103.286
	h_c[a]	0.148689	0.147805	0.140066	0.131109	0.114312
	h_c[b]	0.133623	0.132151	0.127387	0.120693	0.109561
	h_c[c]	0.133199	0.131992	0.127041	0.120507	0.109307
$m = 1$[d]	S	−4.05193	−17.5690	28.6447	28.5096	28.5096
	a	0.785586	0.275882	0.121543	0.121519	0.121519
	$\dot{h}_h$	0.0504910	0.0146159	3.30580×10^{-5}	1.00001×10^{-9}	0.00000
	E	102.344	102.049	106.727	106.747	106.748
	h_c[a]	0.281310	0.0987905	0.0435233	0.0435147	0.0435147
	h_c[b]	0.601459	0.192486	0.0449224	0.0446693	0.0446693
	h_c[c]	0.417985	0.139374	0.0448022	0.0446693	0.0446693
$m = 5$[d]	S	−58.8374	−286.578	70.5775	28.6035	28.5096
	a	0.493256	0.397766	0.217058	0.121649	0.121519
	$\dot{h}_h$	5.26602×10^{-3}	2.97075×10^{-3}	1.35160×10^{-3}	2.29830×10^{-5}	0.00000
	E	98.8249	100.656	100.169	106.634	106.748
	h_c[a]	0.176630	0.142436	0.0777262	0.0435613	0.0435147
	h_c[b]	0.186006	0.144503	0.0805077	0.0448590	0.0446693
	h_c[c]	0.166871	0.133708	0.0755962	0.0447755	0.0446693

Input $E = 100$, $\dot{P}_u = -0.2$ in all cases. Arbitrary units.
[a] Computed from observed a.
[b] Computed from Oliver–Pharr Eq. (3).
[c] Computed from Eq. (5).
[d] Results from initially flat specimen.

overestimation of h_c by the Oliver–Pharr Eq. (3) is due to creep effects. In other words, at small m values, Eq. (5) can partially but not fully correct for creep effects. At large values of m (say > 30), both Eq. (3) and Eq. (5) underestimate h_c due to the occurrence of pile-up, but the discrepancy with the real h_c is not large.

4. Experimental investigation

In this section, experimental results on amorphous selenium (a-Se) will be presented to illustrate the use of Eqs. (4) and (5). The a-Se sample was prepared by melting a 99.99% pure Se button at 300° C followed by quenching to room temperature to avoid crystallization. The as-quenched state already had a surface smooth enough for indentation, and so no extra surface treatment was performed. The indentation experiments were carried out on a nanohardness tester supplied by CSM Instruments SA (Peseux, Switzerland). A simple heating facility was constructed by housing the nanohardness tester in an enclosed chamber with high-power light bulbs inside. When the light bulbs are turned on, a constant temperature of up to ~40 °C

Table 2
Computed finite-element results at different stress exponents

m	1	5	10	30	50	100
S	−20.9876	−40.0265	−115.708	108.856	98.5339	92.6295
a	0.315393	0.387374	0.394270	0.412507	0.412493	0.412760
$\dot{h}_h$	0.0122893	2.82127×10^{-3}	2.49446×10^{-3}	3.66086×10^{-4}	1.73439×10^{-4}	4.39040×10^{-5}
E	104.544	101.187	99.4163	100.120	100.132	100.074
h_c[a]	0.112939	0.138715	0.141184	0.147714	0.147710	0.147805
h_c[b]	0.195757	0.143420	0.142514	0.134290	0.132950	0.132151
h_c[c]	0.151100	0.133168	0.133450	0.132960	0.132320	0.131992

Input $E = 100$, $\dot{\varepsilon}_o = 10^{-2}$, $\dot{P}_u = -0.2$ in all cases. Same arbitrary units as in Table 1.
[a] Computed from observed a.
[b] Computed from Oliver–Pharr Eq. (3).
[c] Computed from Eq. (5).

Table 3
Computed finite-element results at different unloading rates

$\dot{P}_u$		−0.2	−1	−10	−100
$m = 1$	S	−20.9876	662.416	79.5543	73.1204
	a	0.315393	0.315393	0.315393	0.315393
	$\dot{h}_h$	0.0122893	0.0122939	0.0122893	0.0122893
	E	104.544	104.548	104.547	104.547
	h_c[a]	0.112939	0.112939	0.112939	0.112939
	h_c[b]	0.195757	0.160032	0.151994	0.151190
	h_c[c]	0.151100	0.151101	0.151101	0.151101
$m = 100$	S	92.6295	91.1500	90.8229	90.7903
	a	0.412760	0.41276	0.41276	0.41276
	$\dot{h}_h$	4.39040×10^{-5}	4.39040×10^{-5}	4.39040×10^{-5}	4.39040×10^{-5}
	E	100.074	100.077	100.077	100.077
	h_c[a]	0.147805	0.147805	0.147805	0.147805
	h_c[b]	0.132151	0.132024	0.131995	0.131992
	h_c[c]	0.131992	0.131992	0.131992	0.131992

Input $E = 100$, $\dot{\varepsilon}_o = 10^{-2}$ in all cases. Same arbitrary units as in Table 1.
[a] Computed from observed a.
[b] Computed from Oliver–Pharr Eq. (3).
[c] Computed from Eq. (5).

can be maintained inside the chamber. Higher temperatures are possible by adding more heating elements but this was not done as we are not sure whether the nanoindenter will be damaged at higher temperatures. Moreover, 40 °C is a high enough temperature for a-Se to exhibit significant indentation creep.

To investigate the validity of Eqs. (4) and (5), the load cycles shown in Fig. 6 were used. Here, at each testing temperature, the load history comprising loading and load hold up to the point of unloading was maintained the same. Then in different indentation tests at the same temperature, the unloading rates were set to be different. Since the methods described in Eqs. (2)–(5) are about using the unloading behaviour to infer contact stiffness and size at the onset of, or just prior to, the unloading, the real contact stiffness and contact size in all the different runs shown in Fig. 6 should be the same. The validity of Eqs. (2)–(5) can then be judged by checking whether the contact stiffness and size computed using these equations are indeed constant or not.

Table 4
Computed finite-element results at different input Young's modulus

E		10	100	1000
$m = 1$	S	20.2147	−20.9876	−15.7816
	a	0.471910	0.315393	0.301193
	$\dot{h}_h$	8.39035×10^{-3}	0.0122893	0.0129649
	E	10.5465	104.544	1035.00
	h_c[a]	0.168986	0.112939	0.107854
	h_c[b]	0.225218	0.195757	0.193946
	h_c[c]	0.194729	0.151100	0.146834
$m = 100$	S	10.5320	92.6295	938.086
	a	0.459259	0.412760	0.431123
	$\dot{h}_h$	1.09900×10^{-4}	4.39040×10^{-5}	7.08960×10^{-6}
	E	10.3743	100.074	958.177
	h_c[a]	0.164456	0.147805	0.154381
	h_c[b]	0.165984	0.132151	0.130224
	h_c[c]	0.165585	0.131992	0.130198

$\dot{\varepsilon}_o = 10^{-2}$, $\dot{P}_u = -0.2$ in all cases. Same arbitrary units as in Table 1.
[a] Computed from observed a.
[b] Computed from Oliver–Pharr Eq. (3).
[c] Computed from Eq. (5).

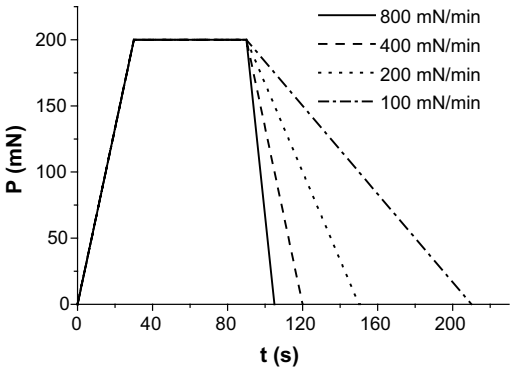

Fig. 6. Typical loading schedules for indentation experiments on a-Se.

Fig. 7 shows the apparent contact stiffness $S = dP/dh$ at the onset of unloading as well as the creep-corrected stiffness calculating using Eq. (4), as a function of the unloading rate. At 19 °C, a "nose" occurs in the load–displacement curve during unloading at 10 mN/min and 50 mN/min, and so the apparent stiffness as shown in Fig. 7(a) is negative at these two unloading rates. At 100 mN/min, no "nose" occurs in the unloading curve but the effect of creep is still very large, so that the apparent stiffness is larger than the elastic value. It is only when the unloading rate is higher than ~500 mN/min that the apparent contact stiffness approaches a constant value as it should be. In Fig. 7(a) is also shown the creep-corrected stiffness calculated using the more general Eq. (16) which can handle the spring-force problem as mentioned in Section 2 above. It can be seen from Fig. 7(a) that the creep-corrected stiffness is all the way constant in all unloading rates studied. This shows that Eq. (4) can effectively correct the creep effects in the contact stiffness. The results at 35 °C as shown in Fig. 7(b) show a similar conclusion. Fig. 8(a) and (b) shows the contact depth h_c calculated using the Oliver–Pharr Eq. (3) as well as the creep-corrected Eq. (5). It can be seen that the

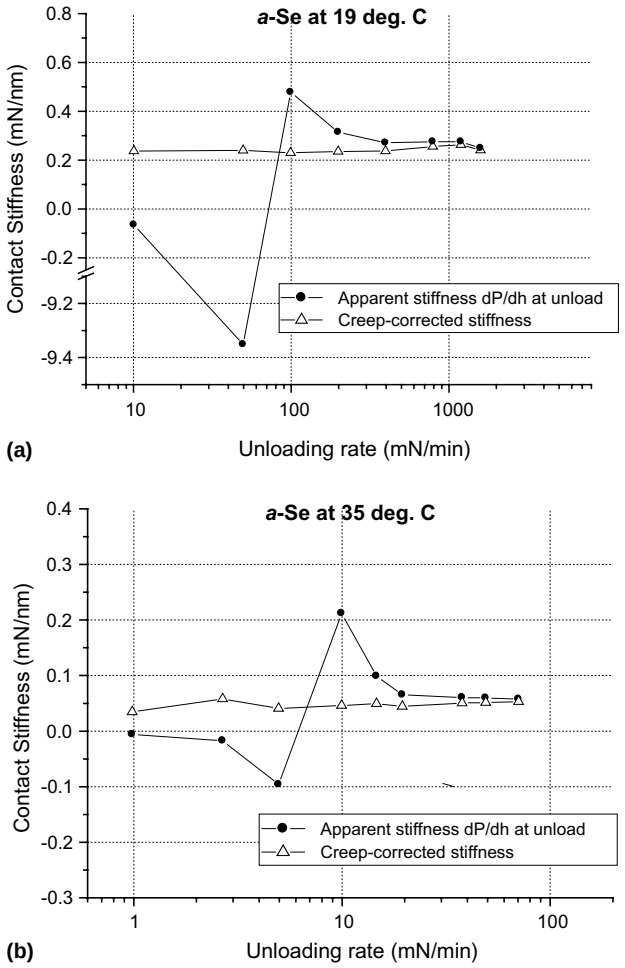

Fig. 7. Effect of unloading rate on apparent and creep-corrected contact stiffness in a-Se at (a) 19 °C with full load 200 mN, (b) 35 °C with full load 5 mN.

Oliver–Pharr equation overestimates the contact size at slow unloading rates at which creep effects are significant. The creep-corrected calculation gives contact depths that are reasonably constant as they should be. Finally, in Fig. 9(a) and (b) are shown the Young's modulus values calculated using the original Oliver–Pharr method, i.e. Eqs. (1)–(3), and the creep-corrected method, i.e., Eqs. (4) and (5). In these calculations, the Poisson's ratio of a-Se was taken to be 0.312 (Etienne et al., 1979). At both 19 °C and 35 °C, the Oliver–Pharr E value becomes negative at small unloading rates because of the negativity of the apparent contact stiffness. At larger unloading rates, the Oliver–Pharr method overestimates the E, and at very fast unloading rates the calculated E value approaches the real value. The creep-correction procedure here can be seen to very effectively produce fairly constant E values. The creep-corrected E here is 8.3 ± 0.3 GPa at 19 °C and 6.0 ± 1.4 at 35 °C. These are in reasonable agreement with the values of ~9.8GPa and ~6.3GPa obtained by ultrasonic measurements at 19 °C and 35 °C respectively (Böhmer and Angell, 1993).

The stress exponent m of our a-Se sample can be obtained from the slope of the log-log plot of the indentation strain rate $\dot{h}/h$ vs stress P/h^2 during load hold (Baker et al., 1992; Li and Ngan, 2004). An example of this is shown in Fig. 10. The m of our a-Se sample is found to be 11.1 ± 1.1 and 3.0 ± 0.2 at 19 °C and 35 °C

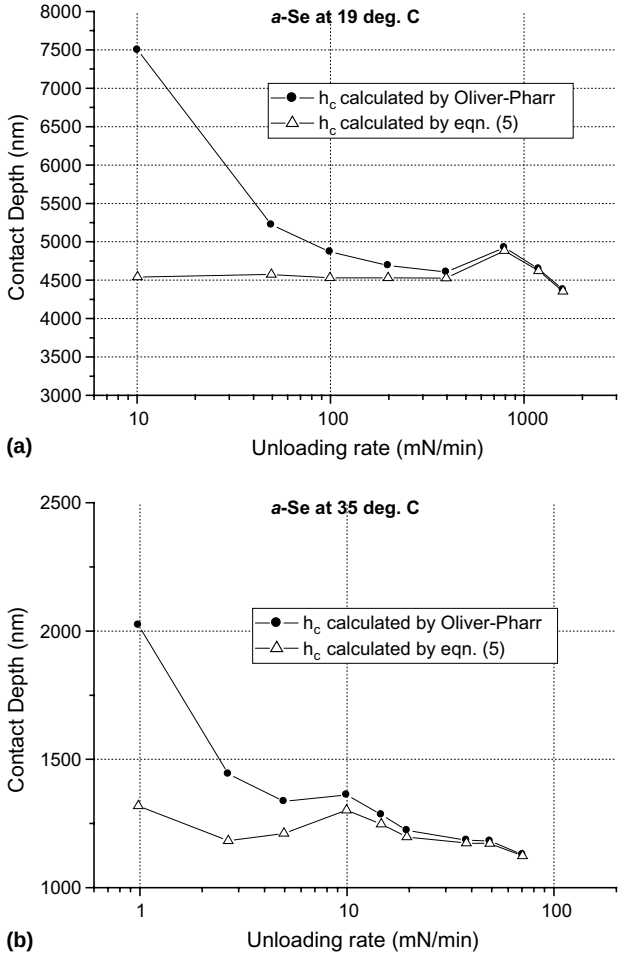

Fig. 8. Effect of unloading rate on calculated contact size in a-Se at (a) 19 °C with full load 200 mN, (b) 35 °C with full load 5 mN.

respectively. It should be noted that the indent sizes at the two temperatures were not the same since the load used and the material behaviour at the two temperatures were not the same. The plastic depths in fact are ~4.5μm and ~ 1.2μm for the loads used at 19 °C and 35 °C respectively, as can be seen from Fig. 8. Li and Ngan (2004) have shown that in a range of materials, the stress exponent exhibits a strong dependence on the indent size, and in general the stress exponent of a smaller indent is lower. In other words, the variation of the stress exponent values here from 3 to 11 for a-Se is likely a combined effect of temperature and size variation. However, the present work is not a systematic attempt to investigate the temperature and size effect of indentation creep in a-Se, although this can be an interesting topic to follow up in the future.

5. Discussion and conclusions

Only experimental results on a-Se were presented in this paper in the interest of space. Experimental results on polypropylene, another rapidly creeping material at room temperature, have already been published elsewhere (Tang and Ngan, 2003), and the conclusions are similar. The present experimental

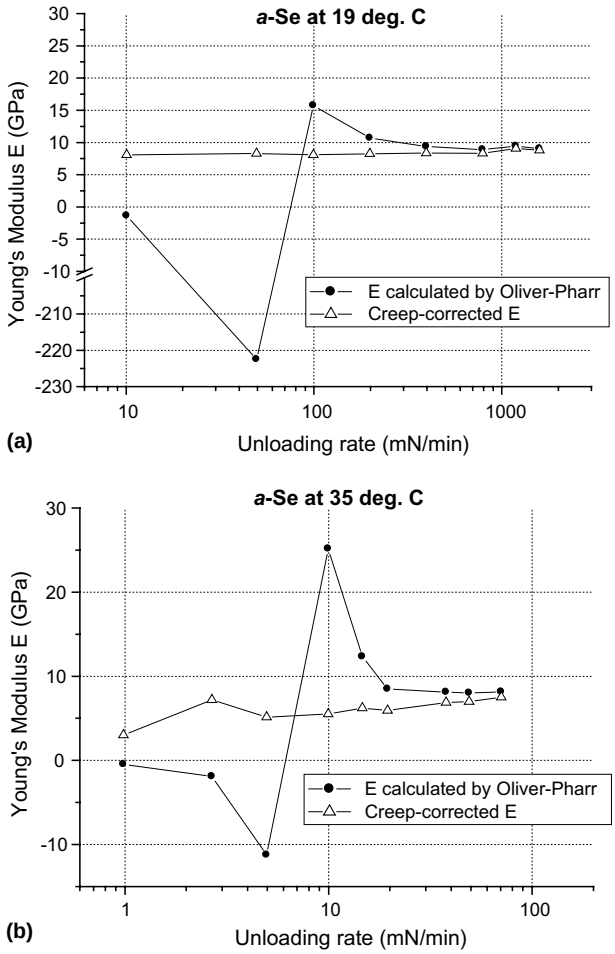

Fig. 9. Effect of unloading rate on calculated Young's modulus in a-Se at (a) 19 °C with full load 200 mN, (b) 35 °C with full load 5 mN.

results in a-Se show that the apparent contact stiffness is subject to severe creep effects at 19 °C or higher temperature. This illustrates that for very soft materials, indentation creep effects may severely influence the accuracy of the measured Young's modulus. Possible materials belonging to this category are biological tissues, polymeric materials, or in fact any material at high enough temperatures. For these, a solution is to do creep correction as stipulated here. For example, the creep correction procedure here has been used successfully to measure the Young's modulus of human dentin (Kinney et al., 2003) and polypropylene (Tang and Ngan, 2003). In the present work, the creep correction procedure has also been found to be effective in a-Se, which is a power-law creeping material with stress exponent of 11 and 3 for the loads used at 19 °C and 35 °C respectively. An alternative solution to eliminate creep effects is to use high-frequency force modulation with a lock-in amplifier to measure the contact stiffness (Oliver and Pethica, 1989). However, the continuous-stiffness function is usually not a standard module in commercial nanoindenters and this usually has to be purchased at an extra cost. The creep correction method here, on the other hand, can be incorporated easily into the data analysis software of a standard machine at minimum cost.

To conclude, the present paper has provided a rigorous proof of a creep-correction formula for calculating the contact stiffness from depth-sensing indentation data, for the Maxwell power-law viscoelastic

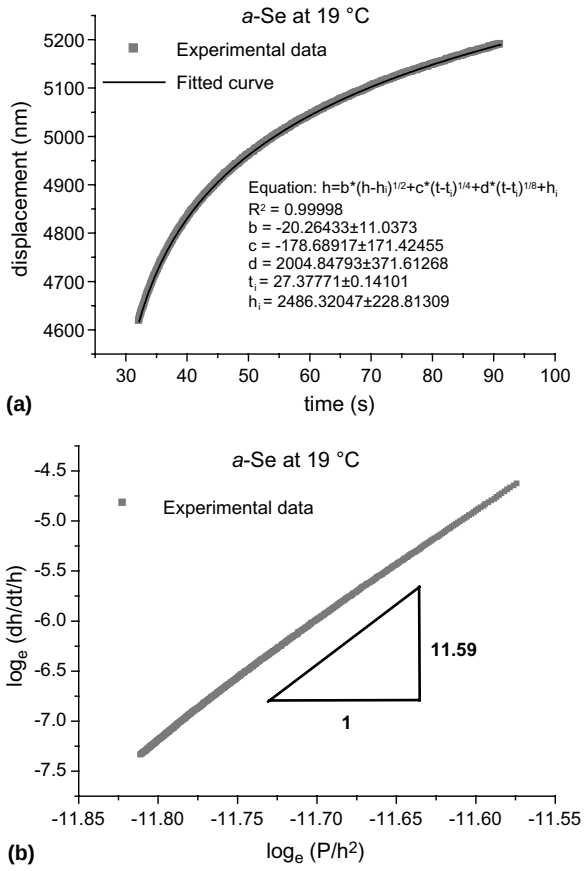

Fig. 10. Determination of stress exponent in a-Se at 19 °C. (a) Displacement (h) vs time (t) curve during load hold at $P = 200$ mN. (b) Log–log plot of indentation strain rate ($\dot{h}/h$) vs (P/h^2) using the data in (a). Here, $\dot{h}(t)$ and $h(t)$ are evaluated using the fitted curve in (a).

material model. Finite-element simulations have confirmed the validity of this correction formula in all the cases simulated. The method was successfully applied to the Young's modulus measurement in a-Se at 19 °C and 35 °C.

Acknowledgment

The work described in this paper was supported by a grant from the Research Grants Council of the Hong Kong Special Administrative Region, People's Republic of China (Project No. HKU 7083/02E). AHWN and HTW also acknowledge financial support from the University of Hong Kong in the form of an Outstanding Young Researcher Award (2001).

References

Baker, S.P., Barbee Jr., T.W., Nix, W.D., 1992. Time-dependent deformation in room-temperature indentation experiments using a nanoindenter. Materials Research Society Symposia Proceedings 239, 319–324.

Böhmer, R., Angell, C.A., 1993. Elastic and viscoelastic properties of amorphous selenium and identification of the phase transition between ring and chain structures. Physical Review B 48, 5857–5864.

Bower, A.F., Fleck, N.A., Needleman, A., Ogbonna, N., 1993. Indentation of a power law creeping solid. Proceedings of the Royal Society of London A 441, 97–123.

Chudoba, T., Richter, F., 2001. Investigation of creep behaviour under load during indentation experiments and its influence on hardness and modulus results. Surface and Coatings Technology 148, 191–198.

Etienne, S., Guenin, G., Perez, J., 1979. Ultrasonic studies of the elastic coefficients of vitreous selenium about T_g. Journal of Physics D 12, 2189–2202.

Feng, G., Ngan, A.H.W., 2001a. Creep and strain burst in indium and aluminium during nanoindentation. Scripta Materialia 45, 971–976.

Feng, G., Ngan, A.H.W., 2001b. The effects of creep on elastic modulus measurement using nanoindentation. Materials Research Society Symposia Proceedings 649, 7.1.1–7.1.6.

Feng, G., Ngan, A.H.W., 2002. Effects of creep and thermal drift on modulus measurement using depth-sensing indentation. Journal of Materials Research 17, 660–668.

Kinney, J.H., Marshall, S.J., Marshall, G.W., 2003. The mechanical properties of human dentin: a critical review and re-evaluation of the dental literature. Critical Review of Oral Biological Medicine 14, 13–29.

LaFontaine, W.R., Yost, B., Black, R.D., Li, C.Y., 1990. Indentation load relaxation experiments with indentation depth in the submicron range. Journal of Materials Research 5, 2100–2106.

Li, H., Ngan, A.H.W., 2004. Size effects of nanoindentation creep. Journal of Materials Research 19, 513–522.

Lucas, B.N., Oliver, W.C., 1999. Indentation power-law creep of high-purity indium. Metallurgical and Materials Transactions 30A, 601–610.

Mayo, M.J., Nix, W.D., 1988. A micro-indentation study of superplasticity in Pb, Sn, and Sn–38 wt.%Pb. Acta Metallurgica et Materialia 36, 2183–2192.

McElhaney, K.W., Vlassak, J.J., Nix, W.D., 1998. Determination of indenter tip geometry and indentation contact area for depth-sensing indentation experiments. Journal of Materials Research 13, 1300–1306.

Ngan, A.H.W., Tang, B., 2002. Viscoelastic effects during unloading in depth-sensing indentation. Journal of Materials Research 17, 2604–2610.

O'Connor, K.M., Cleveland, P.A., 1993. Indentation creep studies of cross-linked glassy polymer films. Materials Research Society Symposia Proceedings 308, 495–502.

Oliver, W.C., Pethica, J.B., 1989. Method for continuous determination of the elastic stiffness of contact between two bodies. United States Patent No. 4,848,141.

Oliver, W.C., Pharr, G.M., 1992. An improved technique for determining hardness and elastic modulus using load and displacement sensing indentation experiments. Journal of Materials Research 7, 1564–1583.

Pharr, G.M., Olive, W.C., Brotzen, F.R., 1992. On the generality of the relationship among contact stiffness, contact area, and elastic modulus during indentation. Journal of Materials Research 7, 613–617.

Raman, V., Berriche, R., 1992. An investigation of the creep processes in tin and aluminium using a depth-sensing indentation technique. Journal of Materials Research 7, 627–638.

Sakai, M., 2002. Time-dependent viscoelastic relation between load and penetration for an axisymmetric indenter. Philosophical Magazine A 82, 1841–1849.

Sneddon, I.N., 1965. The relation between load and penetration in the axisymmetric Boussinesq problem for a punch of arbitrary profile. International Journal of Engineering Science 3, 47–57.

Syed, S.A., Pethica, J.B., 1997. Nanoindentation creep of single-crystal tungsten and gallium arsenide. Philosophical Magazine A 76, 1105–1118.

Tang, B., Ngan, A.H.W., 2003. Accurate measurement of tip–sample contact size during nanoindentation of viscoelastic materials. Journal of Materials Research 18, 1141–1148.